Journal of Mathematical Modeling
Vol. 12, No. 1, 2024, pp. 99–115. Research Article

JMM

A fifth-order symmetrical weighted hybrid ENO-flux limiter scheme for traffic flow model on networks

Rooholah Abedian*

School of Engineering Science, College of Engineering, University of Tehran, Iran
Email(s): rabedian@ut.ac.ir

Abstract. In this research work, a fifth-order weighted essentially non-oscillatory (WENO) scheme is created for traffic flow problems on networks. Street systems can be numerically demonstrated as a graph, whose edges are a limited number of streets that connect at intersections. A scalar hyperbolic conservation law can portray the advancement on each street, and traffic distribution matrices are considered to define coupling conditions at the network intersections. In this paper, numerical results for road networks with rich solution structures will be presented. These numerical results show that the new proposed scheme in this paper can generate essentially non-oscillatory and high resolution solutions.

Keywords: Finite volume scheme, traffic flow, WENO scheme.
AMS Subject Classification 2010: 35R11, 65M06.

1 Introduction

By utilizing partial differential equations (PDEs), microscopic model of traffic flow endeavours to demonstrate the advancement of the vehicular traffic density. Authors of [11, 15] proposed a simple first order fluid approximation of traffic flow dynamics to describe the evolution of traffic flow on a single road. Nowadays, this classical Lighthill-Whitham-Richards (LWR) model is the basis of many fluid-dynamic models for traffic flow. Authors of [16] developed a multi-class model with heterogeneous drivers. In [6], a macroscopic behavioural theory of traffic dynamics for homogeneous, multi-lane free-ways was developed. For traffic flow on road networks, a number of different models such as [5, 7, 9] have been developed. On each road, the traffic network can be described by employing PDEs, specifically conservation laws, at the macroscopic scale.

The traditional LWR PDE is a scalar hyperbolic conservation law. Thus, it can be numerically solved by variety of numerical methods, such as Godunov's scheme and first-order Lax-Friedrichs finite

*Corresponding author
Received: 14 July 2023 / Revised: 22 September 2023 / Accepted: 27 November 2023
DOI: 10.22124/jmm.2023.24976.2220

difference scheme. Also, for solving multi-class models, the first-order Lax-Friedrichs finite difference scheme can be employed. Using classical first order Godunov scheme and kinetic schemes, numerical solutions to traffic flow problems on road networks are obtained in [2]. In recent years, a number of high-order methods were developed for solving continuum traffic flow models. In [17], a high-order WENO scheme for solving a multi-class LWR model has been developed. The numerical results, reported in [17], demonstrate that the weighted essentially non-oscillatory (WENO) scheme is more efficient than the low-order Lax-Friedrichs scheme. Also, WENO scheme was employed to solve a multi-class traffic flow model with spatially varying fluxes for an inhomogeneous highway [18]. In [12], to model the asymmetry in traffic flow, the WENO approach was employed.

Recently, many high-order finite difference or finite volume numerical schemes have been developed for hyperbolic conservation laws. The essentially non-oscillatory (ENO) and WENO schemes, which have been employed quite successfully to solve the problems with strong shocks, contact discontinuities and sophisticated smooth structures, are the primary schemes used as the current state of the art in the literature. The first WENO scheme was originally proposed by Liu, Osher and Chan [13], in which instead of using the optimal smooth candidate stencil for the reconstruction of high-order ENO type schemes, a linear convex combination of all stencils including non-smooth stencils is used. After that, such WENO scheme was improved by Jiang and Shu [10], in which a general framework for the designing of new smoothness indicators and non-linear weights was specified in detail.

In this paper, we propose to apply a hybrid WENO (HyWENO) scheme for simulating hyperbolic road network problems. The main procedure of HyWENO scheme is given in the following. First, in the finite volume framework, a polynomial based on the cell averages is reconstructed in the interval of the big spatial stencil. Second, the location of the extreme points of the reconstructed polynomial is identified. Third, if the extreme points of the reconstruction polynomial in the big spatial stencil are located outside of the same stencil, the reconstructed polynomial is adapted to approximate the numerical flux straightforwardly. This approximation is of high-order accuracy, resulting in a linear upwind scheme with fewer numerical errors. Otherwise, the symmetrical weighted hybrid ENO-flux limiter reconstruction procedure [1] is applied to reconstruct the numerical flux.

The rest of this paper is organized as follows. In Section 2, the class of traffic models on networks under consideration is reviewed. The finite volume HyWENO scheme for the governing equation for the first-order LWR model in one dimension are introduced in Section 3. In Section 4, the numerical results for some network problems are demonstrated. Concluding remarks are prepared in Section 5.

2 Macroscopic traffic models

In a single road, we can describe the non-linear LWR model based on the conservation of cars by a scalar hyperbolic conservation law as follows

$$\rho_t + f(\rho)_x = 0, \tag{1}$$

where $\rho = \rho(x,t) \in [0, \rho_{\max}]$ is the density of cars at time t, with $\rho_{\max} > 0$ is the maximum density of cars. The function $f(\rho) = \rho v$ is the flux, where we can suppose that v is a given smoothing decreasing function of density, depending only on the density. Other assumptions about flux f are $f(0) = f(\rho_{\max}) = 0$ and it is strictly concave.

In this research work, a road network introduced in [3] is considered. Accordingly, there are finite number of roads $[a_i, b_i]$ that meet at some junctions. Consider a junction J with incoming roads $\mathscr{I}_i$,

where $i = 1,\dots,n$ and outgoing roads $\mathscr{I}_j$ with $j = n+1,\dots,n+m$. The choice of the outgoing road is prescribed by traffic distribution matrix [3]

$$\mathbf{A} = \begin{bmatrix} \alpha_{n+1,1} & \dots & \alpha_{n+1,n} \\ \vdots & \ddots & \vdots \\ \alpha_{n+m,1} & \dots & \alpha_{n+m,n} \end{bmatrix}.$$

Here, $\alpha_{j,i}$ is the the percentage of traffic coming from the incoming road i and going to the outgoing road j. The conservation of vehicles requires that the total inflow into the junction equals the total outflow out of the junction as follows

$$\sum_{i=1}^{n} f(\rho_i(b_i,t)) = \sum_{j=n+1}^{n+m} f(\rho_j(a_j,t)), \tag{2}$$

where ρ_i with $i = 1,\dots,n$ are the car densities on incoming roads; ρ_j with $j = n+1,\dots,n+m$ are the car densities on outgoing roads. The following three rules are considered to determine a unique solution to Riemann problems at junctions [4]:

- The i-th column of matrix $\mathbf{A}$ satisfies $\sum_{j=n+1}^{n+m} \alpha_{j,i} = 1$.
- Respecting the previous rule, the maximization of the flux is imposed through the junction. If $n > m$, then the next rule is needed.
- To illustrate this case, two incoming roads a and b and one outgoing road c are considered. If not all incoming cars can enter the outgoing road c, and let Q be the quantity that can enter the outgoing road. Then qQ cars come from first incoming road a and $(1-q)Q$ cars from another, where $0 \le q \le 1$ is a right of way parameter.

The initial densities at junction J are demonstrated by $\rho_{k,0}$ with $k = 1,2,\dots,n+m$. The maximum fluxes that can be obtained on incoming and outgoing roads are represented by $\gamma_i^{\max}$ with $i = 1,\dots,n$ and $\gamma_j^{\max}$ with $j = n+1,\dots,n+m$, respectively, that they can be defined as [4]

$$\gamma_i^{\max} = \begin{cases} f(\rho_{i,0}), & \rho_{i,0} \in [0,\xi], \\ f(\xi), & \rho_{i,0} \in [\xi,\rho_{\max}], \end{cases} \qquad \gamma_j^{\max} = \begin{cases} f(\xi), & \rho_{j,0} \in [0,\xi], \\ f(\rho_{j,0}), & \rho_{j,0} \in [\xi,\rho_{\max}], \end{cases} \tag{3}$$

where ξ is a strict maximum, such that $f'(\xi) = 0$. It can be concluded that the flux in incoming road at junctions must be equal to or less than the demand flux $f(\xi)$. It seems that there are infinitely many possible new fluxes that can be obtained based condition (3). Accordingly, in this research work, traffic network with different arcs and one junction is considered as shown in [4].

3 Hybrid WENO scheme with maximum-principle-preserving limiter

This section briefly describes how to design HyWENO scheme for 1D traffic flow models in a single road. In [1], Abedian et al. developed a finite volume symmetrical WENO scheme for solving conservation laws. First, a HyWENO scheme is developed for the non-linear model in a single road (1), then the scheme is extended to 1D network problems. We consider an uniform grid on computational domain $[a_i,b_i]$ with cells $I_j = [x_{j-\frac{1}{2}},x_{j+\frac{1}{2}}], j = 1,\dots,N$. The cell-averaged value $\bar{\rho}_j$ is defined in the following form

$$\bar{\rho}_j(t) = \frac{1}{\Delta x}\int_{I_j} \rho(x,t)dx. \tag{4}$$

The classical finite volume scheme for (1) can be written as

$$\frac{d}{dt}\bar{\rho}_j(t) = -\frac{1}{\Delta x}(\hat{f}_{j+\frac{1}{2}} - \hat{f}_{j-\frac{1}{2}}), \tag{5}$$

with a global Lax-Friedrichs flux defined by

$$\hat{f}_{j+\frac{1}{2}} = h(\rho^-_{j+\frac{1}{2}}, \rho^+_{j+\frac{1}{2}}) = \frac{1}{2}\left[f(\rho^+_{j+\frac{1}{2}}) + f(\rho^-_{j+\frac{1}{2}}) - \alpha(\rho^-_{j+\frac{1}{2}} - \rho^+_{j+\frac{1}{2}})\right], \tag{6}$$

where $\alpha = \max_\rho |f'(\rho)|$, $\rho^-_{j+\frac{1}{2}}$ and $\rho^+_{j+\frac{1}{2}}$ are approximated by a high-order HyWENO reconstruction, which will now be discussed.

3.1 The HyWENO scheme

Step 1. By considering the big stencil $S = \{I_{j-2}, \ldots, I_{j+2}\}$, the fourth degree reconstruction polynomial p can be easily obtained by making the following condition

$$\frac{1}{\Delta x}\int_{I_i} p(\eta)\mathrm{d}\eta = \bar{\rho}_i, \quad i = j-2, \ldots, j+2. \tag{7}$$

Step 2. Identify the extreme points of $p(x)$. Since the degree of $p'(x)$ is at most three, therefore, the real zero points of $p'(x)$ can be explicitly solved and one is the extreme point of $p(x)$ if it is not a doubled zero point of $p'(x)$.

Step 3. Now if the extreme points of the reconstruction polynomial $p(x)$ are outside of the big stencil S or there is no extreme point at all, the approximations at the boundaries of each cell are directly given by $\rho^-_{j+\frac{1}{2}} := \rho^{-up}_{j+\frac{1}{2}} = p(x_{j+\frac{1}{2}})$ and $\rho^+_{j-\frac{1}{2}} := \rho^{+up}_{j-\frac{1}{2}} = p(x_{j-\frac{1}{2}})$ and the procedure jumps to step 5.

Step 4. Now if there is one or more extreme points in the big stencil S, the WENO process proposed by Abedian et al. [1] is applied to approximate $\rho^\pm_{j\mp\frac{1}{2}}$ as follows. The big stencil S is divided into three smaller stencils $S_0 = \{I_{j-2}, I_{j-1}, I_j\}$, $S_1 = \{I_{j-1}, I_j, I_{j+1}\}$ and $S_2 = \{I_j, I_{j+1}, I_{j+2}\}$ whose community is the same S. Now we need three reconstruction polynomials $p_r(x)$, $r = 0, 1, 2$ associated to these small stencils. First we find the polynomial $\mathscr{P}_r(x)$ from cell boundaries of the stencil S_r

$$\mathscr{P}_r(x) = \sum_{i=1}^{3} U[x_{j-r-\frac{1}{2}}, \ldots, x_{j-r+i-\frac{1}{2}}] \sum_{m=0}^{i-1} \prod_{l=0, l\neq m}^{i-1} (x - x_{j-r+l-\frac{1}{2}}), \tag{8}$$

where $U[\cdots]$ is a divided difference of the function $U(x) = \int_{-\infty}^{x} \rho(\xi, t)d\xi$. In order to achieve more efficient reconstruction than ENO3 reconstruction (8), initially, a random point labelled as x_{j+ar+b} is selected and then a Taylor series expansion is utilized to determine the point that yields the greatest accuracy. Consequently, we deduce that a and b are both equal to zero. Therefore, the point x_j is added to interpolation (8),

$$p_r(x) = \mathscr{P}_r(x) + U[x_{j-r-\frac{1}{2}}, \ldots, x_{j-r+\frac{5}{2}}, x_j] \sum_{m=0}^{3} \prod_{l=0, l\neq m}^{3} (x - x_{j-r+l-\frac{1}{2}}), \quad r = 0, 1, 2. \tag{9}$$

Remark 1. *From (9), it is evident that the polynomial $p_r(x)$ is a cubic polynomial, meaning it has a degree of three. As a result, the reconstruction described in Eq. (9) is capable of precisely reproducing polynomials of degree three within the stencil. The objective of polynomials of the form (8) and (9) is to approximate the boundaries of cell I_j. By incorporating additional information within cell I_j, we aim to utilize data that is closer to the centre of the cell, as opposed to data that is farther away. This approach allows for a more accurate representation of the cell boundaries. The polynomial (9) interpolates a greater number of points, which aids in approximating the cell boundaries more effectively. When the reconstruction is smooth, meaning there are no abrupt changes or discontinuities, we can achieve higher levels of accuracy. Additionally, there is an expectation that the polynomial satisfies the conservation property, ensuring that important quantities such as mass, momentum, or energy are preserved accurately during the approximation process.*

The divided difference $U[x_{j-r+\frac{5}{2}},x_j]$ of Eq. (9) is calculated by

$$U[x_{j-r+\frac{5}{2}},x_j]=\frac{1}{\mathscr{A}}\left[\int_{-\infty}^{x_j}\rho(\xi)d\xi-\int_{-\infty}^{x_{j-r+\frac{5}{2}}}\rho(\xi)d\xi\right]=\frac{1}{\mathscr{A}}\int_{x_{j-r+\frac{5}{2}}}^{x_j}\sum_j L_j(x)\chi_j(x)dx, \tag{10}$$

where $\mathscr{A}=x_j-x_{j-r+\frac{5}{2}}$ and $\chi_j(x)$ is the characteristic function of the cell I_j. To complete Eq. (10), a polynomial is needed that retains the information in the cell I_j, therefore, similar to the NT scheme [14], the polynomial $L_j(x)=\bar{\rho}_j+(x-x_j)\frac{1}{\Delta x}\rho'_j$ is applied, where the numerical derivative ρ'_j is obtained by the UNO limiter [8]. By placing $L_j(x)$ in Eq. (10), the following equation is explicitly obtained

$$U[x_{j-r+\frac{5}{2}},x_j]=\frac{1}{5-2r}(\bar{\rho}_j-(r^2-r-2)\bar{\rho}_{j+1}+(r^2-3r+2)\bar{\rho}_{j+2}+\frac{1}{4}\rho'_j),\quad r=0,1,2, \tag{11}$$

accordingly, we can obtain

$$\begin{aligned}
\rho^{-(0)}_{j+\frac{1}{2}}&:=p_0(x_{j+\frac{1}{2}})=(22\bar{\rho}_j+9\bar{\rho}_{j+1}-\bar{\rho}_{j+2}+8\rho'_j)/30,\\
\rho^{-(1)}_{j+\frac{1}{2}}&:=p_1(x_{j+\frac{1}{2}})=(\bar{\rho}_{j-1}+15\bar{\rho}_j+2\bar{\rho}_{j+1}+8\rho'_j)/18,\\
\rho^{-(2)}_{j+\frac{1}{2}}&:=p_2(x_{j+\frac{1}{2}})=(-2\bar{\rho}_{j-2}+13\bar{\rho}_{j-1}+19\bar{\rho}_j+24\rho'_j)/30,
\end{aligned} \tag{12}$$

and

$$\begin{aligned}
\rho^{+(0)}_{j-\frac{1}{2}}&:=p_0(x_{j-\frac{1}{2}})=(19\bar{\rho}_j+13\bar{\rho}_{j+1}-2\bar{\rho}_{j+2}-24\rho'_j)/30,\\
\rho^{+(1)}_{j-\frac{1}{2}}&:=p_1(x_{j-\frac{1}{2}})=(2\bar{\rho}_{j-1}+15\bar{\rho}_j+\bar{\rho}_{j+1}-8\rho'_j)/18,\\
\rho^{+(2)}_{j-\frac{1}{2}}&:=p_2(x_{j-\frac{1}{2}})=(-\bar{\rho}_{j-2}+9\bar{\rho}_{j-1}+22\bar{\rho}_j-8\rho'_j)/30.
\end{aligned} \tag{13}$$

The reconstruction

$$\rho^{\pm(3)}_{j\mp\frac{1}{2}}:=\frac{1}{d_3}[\rho^{\pm up}_{j\mp\frac{1}{2}}-\sum_{k=0}^{2}d_k\rho^{\pm(k)}_{j\mp\frac{1}{2}}],$$

is also considered to obtain symmetrical linear weights d_r. In the small stencils S_r, if there is large gradients or discontinuities, the related reconstructions produce spurious oscillations, so to prevent or

minimize this, the *smoothness indicator* β_r associated with each stencil is introduced as follows

$$\beta_r = \sum_{k=1}^{2} \Delta x^{2k-1} \int_{I_j} \left(\frac{d^k}{dx^k} p_r(x) \right)^2 \mathrm{d}x, \; r = 0,1,2. \tag{14}$$

Practically, the definition of β_3 may be simplified by using $\max(\beta_0, \beta_1, \beta_2)$ instead. A direct computation based on (9) yields:

$$\begin{aligned} \beta_r = & \frac{1}{8100}(9\bar{\rho}_j - 12\bar{\rho}_{j+(1-r)} + 3\bar{\rho}_{j+2(1-r)} + (1-r)96\rho'_j)^2 \\ & + \frac{13}{2700}(57\bar{\rho}_j - 66\bar{\rho}_{j+(1-r)} + 9\bar{\rho}_{j+2(1-r)} + (1-r)48\rho'_j)^2 \\ & + \frac{781}{162000}(72\bar{\rho}_j - 96\bar{\rho}_{j+(1-r)} + 24\bar{\rho}_{j+2(1-r)} + (1-r)48\rho'_j)^2, \quad r = 0,2, \end{aligned} \tag{15}$$

and

$$\begin{aligned} \beta_1 = & \frac{9}{2916}(\bar{\rho}_{j-1} - \bar{\rho}_{j+1} - 16\rho'_j)^2 + \frac{13}{12}(\bar{\rho}_{j-1} - 2\bar{\rho}_j + \bar{\rho}_{j+1})^2 \\ & + \frac{449856}{58320}(\bar{\rho}_{j-1} - \bar{\rho}_{j+1} + 2\rho'_j)^2. \end{aligned} \tag{16}$$

Therefore, the non-linear weights based on the linear weights d_r and associated smoothness indicators are obtained as [10]

$$\omega_r = \frac{\alpha_r}{\sum_{k=0}^{3} \alpha_k}, \quad \alpha_l = \frac{d_l}{(\varepsilon + \beta_l)^2}, \quad r,l = 0,1,2,3. \tag{17}$$

Here, ε is a positive constant that is used to prevent division by zero, thus ε is set as 10^{-6}. For linear weights any convex combination can be considered. Accordingly, we make the choice: $d_0 = d_2 = \frac{1}{8}, d_1 = \frac{1}{4}, d_3 = \frac{1}{2}$. Therefore, the final approximations at the boundaries of each cell are given by

$$\rho^-_{j+\frac{1}{2}} = \sum_{i=0}^{3} \omega_i \rho^{-(i)}_{j+\frac{1}{2}}, \qquad \rho^+_{j-\frac{1}{2}} = \sum_{i=0}^{3} \omega_i \rho^{+(i)}_{j-\frac{1}{2}}. \tag{18}$$

Step 5. The semi-discrete scheme (5) is discretized in time by a third-order strong stability preserving (SSP) high-order Runge-Kutta (RK) time discretizations in the following form [10]

$$\begin{aligned} \rho_j^{(1)} &= \rho_j^n + \Delta t F(\rho_j^n), \\ \rho_j^{(2)} &= \tfrac{3}{4}\rho_j^n + \tfrac{1}{4}\rho_j^{(1)} + \tfrac{1}{4}\Delta t F(\rho_j^{(1)}), \\ \rho_j^{n+1} &= \tfrac{1}{3}\rho_j^n + \tfrac{2}{3}\rho_j^{(2)} + \tfrac{2}{3}\Delta t F(\rho_j^{(2)}), \end{aligned} \tag{19}$$

where $F(\rho)$ is the spatial operator.

3.2 Maximum-principle-satisfying limiter

For scalar hyperbolic conservation laws (1), the forward Euler temporal discretization for the semi-discrete scheme (2) is

$$\bar{\rho}_j^{n+1} = \bar{\rho}_j^n - \lambda \left(h(\rho^-_{j+\frac{1}{2}}, \rho^+_{j+\frac{1}{2}}) - h(\rho^-_{j-\frac{1}{2}}, \rho^+_{j-\frac{1}{2}}) \right), \tag{20}$$

where $\lambda = \frac{\Delta t}{\Delta x}$. Also, $\rho^{\pm}_{j+\frac{1}{2}}$ are reconstructed from HyWENO scheme, discussed in the previous subsection. The maximum-principle-satisfying polynomial rescaling limiter proposed in [19] can be written as

$$\tilde{p}(x) = \theta(p(x) - \bar{\rho}_j) + \bar{\rho}_j, \quad \theta = \min\left\{ \left| \frac{\rho_{\max} - \bar{\rho}^n_j}{M_j - \bar{\rho}^n_j} \right|, \left| \frac{\bar{\rho}^n_j}{m_j - \bar{\rho}^n_j} \right|, 1 \right\}. \tag{21}$$

Here, M_j and m_j are the maximum and the minimum of $p(x)$ at Legendre Gauss-Lobatto quadrature points for the cell I_j. It can be easily checked that with the application of such a limiter, the conservation and bound preserving properties of the numerical solution are satisfied. Furthermore, it was proved [19] that such a limiting process maintains the original order accuracy of the approximation. Hence (20) can be rewritten as

$$\bar{\rho}^{n+1}_j = \bar{\rho}^n_j - \lambda \left(h(\tilde{\rho}^-_{j+\frac{1}{2}}, \tilde{\rho}^+_{j+\frac{1}{2}}) - h(\tilde{\rho}^-_{j-\frac{1}{2}}, \tilde{\rho}^+_{j-\frac{1}{2}}) \right), \tag{22}$$

where $\tilde{\rho}^+_{j-\frac{1}{2}} = \tilde{p}(x_{j-\frac{1}{2}})$ and $\tilde{\rho}^-_{j+\frac{1}{2}} = \tilde{p}(x_{j+\frac{1}{2}})$, it was proven that the scheme (22) satisfies a strict maximum principle for scalar conservation laws under the CFL condition

$$\lambda \alpha \leq \frac{1}{12}, \tag{23}$$

with a global Lax-Friedrichs flux. Because SSP high order RK time discretization (19) is a convex combination of Euler forward, HyWENO scheme with this time discretization will still satisfy the maximum principle [19].

4 Numerical results

In this section, some benchmark test cases are employed to check the proposed high-order finite volume hybrid WENO, named as "HyWENO" scheme. The reference solution generated by the traditional fifth-order WENO scheme of Jiang and Shu (WENO-JS) [10] with $N = 5000$ grid points is denoted as "Reference". For all the numerical test cases, the third-order SSP RK method (19) is considered under the CFL condition (23).

4.1 Accuracy test

The first test is to solve the traffic flow Eq. (1) with the following flux function

$$f(\rho) = \rho(1-\rho), \quad \rho \in [0,1], \tag{24}$$

with the initial condition $\rho(x,0) = 0.5 + 0.5\sin(2\pi x)$. The computational domain is $[0,1]$ and the periodic boundary condition is assigned. The solution up to time $T = 0.1$ is computed. The results are shown in Table 1. One can observe the fifth-order convergence rate for HyWENO scheme. The HyWENO scheme is also tested with the following initial condition,

$$\rho(x,0) = \begin{cases} 1, & x \in [0,0.3] \cup [0.6,1], \\ 0, & \text{otherwise.} \end{cases} \tag{25}$$

The numerical solutions of HyWENO scheme with limiter, WENO-JS scheme with limiter, HyWENO without limiter, named as "HyWENO-without" and the "Reference" solution are demonstrated in Fig. 1. As can be seen, HyWENO scheme with limiter presents better resolution than the traditional WENO schemes.

Table 1: Errors and orders of convergence for "accuracy test" with $\rho(x,0) = 0.5 + 0.5\sin(2\pi x)$.

	HyWENO				WENO-JS			
N	L_1-error	L_1-order	L_∞-error	L_∞-order	L_1-error	L_1-order	L_∞-error	L_∞-order
10	1.64E-02	-	5.31E-02	-	1.90E-02	-	7.49E-02	-
20	1.45E-03	3.51	9.75E-03	2.45	2.03E-03	3.20	1.22E-02	2.64
40	7.30E-05	4.31	6.91E-04	3.81	1.23E-04	4.06	1.04E-03	3.55
80	2.39E-06	4.94	3.05E-05	4.50	4.46E-06	4.83	4.73E-05	4.47
160	7.05E-08	5.08	9.32E-07	5.04	1.63E-07	4.75	1.37E-06	5.08
320	2.09E-09	5.08	2.77E-08	5.06	4.74E-09	5.10	7.29E-08	4.26

4.2 Bottleneck

The simplest traffic flow model on networks is represented by the bottleneck problem. The conservation of cars is always expressed by (1), supplemented with initial and boundary conditions. The bottleneck problem models a road with different widths, hence different flux functions along different parts of the road are needed. The coupling conditions at junction with one incoming road a and one outgoing road b are set to be

$$\hat{\gamma}_a = \hat{\gamma}_b = \hat{\gamma}, \quad \hat{\gamma} = \min\{\gamma_a^{\max}, \gamma_b^{\max}\}. \tag{26}$$

Here, $\gamma_a^{\max}$ and $\gamma_b^{\max}$ are determined in (3). Accordingly, the numerical fluxes of the junction point at incoming and outgoing roads are taken as

$$\hat{f}^a_{N+\frac{1}{2}} = \hat{\gamma}_a, \quad \hat{f}^b_{\frac{1}{2}} = \hat{\gamma}_b. \tag{27}$$

The flux function $f_1(\rho)$ in the widest road a is given by Eq. (24), while the flux function in the narrowest road b

$$f_2(\rho) = \rho(1 - \frac{3}{2}\rho), \quad \rho \in [0, \frac{2}{3}].$$

The maximum of the fluxes is unique:

$$f_1(\xi_1) = \max_{[0,1]} f_1(\rho) = \frac{1}{4}, \ \ \xi_1 = \frac{1}{2}; \quad f_2(\xi_2) = \max_{[0,\frac{2}{3}]} f_2(\rho) = \frac{1}{6}, \ \ \xi_2 = \frac{1}{3}.$$

Let ρ_l be the traffic density for the incoming road a and ρ_r be the traffic density for the outgoing road b. We first consider the following initial and boundary data:

$$\begin{aligned} &\rho_1(x,0) = 0.66, \ x \in [0,1], \\ &\rho_2(x,0) = 0.66, \ x \in [1,2], \\ &\rho_1(0,t) = \rho_{1,b}(t) = 0.25, \ t > 0. \end{aligned} \tag{28}$$

The initial value 0.66 is very close to the maximum value that can be absorbed by road b, after a short time, e.g. $T = 0.5$, the formation of a traffic jam can be observed, see Fig. 2.

We then consider the following initial and boundary data:

$$\begin{aligned} &\rho_1(x,0) = 0, \ x \in [0,1], \\ &\rho_2(x,0) = 0, \ x \in [1,2], \\ &\rho_1(0,t) = \rho_{1,b}(t) = 0.4, \ t > 0. \end{aligned} \tag{29}$$

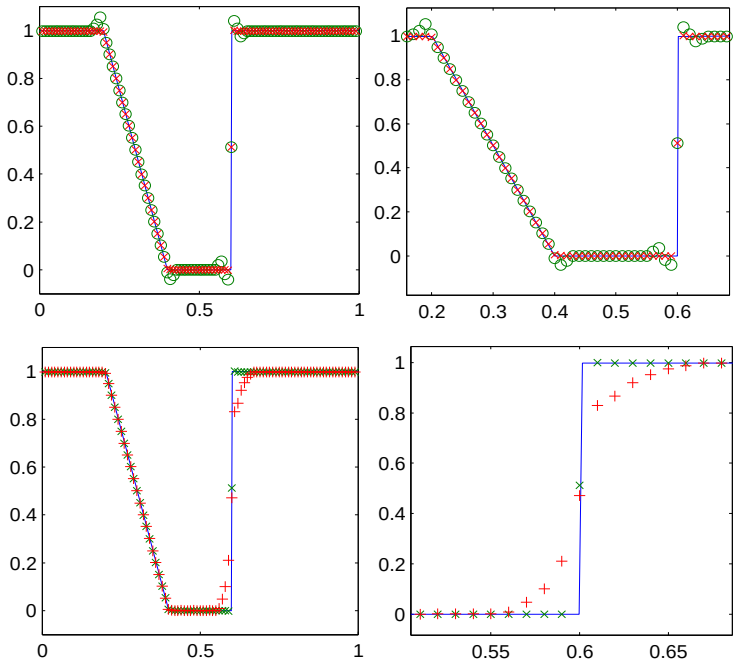

Figure 1: Accuracy test with initial data (25). Left: numerical solution with $N = 100$ at the final time $T = 0.1$. Right: Zoomed region. HyWENO-without: "$\circ$", HyWENO: "$\times$" and WENO-JS: "$+$".

Since $\rho_{1,b} > \bar{\rho} \approx 0.21$, there is a jam formation as showed by Fig. 3. The results obtained here are comparable with those in [2].

Finally, we consider the following initial and boundary data:

$$\begin{aligned} &\rho_1(x,0) = 0.4 + 0.2\sin(5\pi x),\ x \in [0,1], \\ &\rho_2(x,0) = 0.66,\ x \in [1,2], \\ &\rho_1(0,t) = \rho_{1,b}(t) = 0.25,\ t > 0. \end{aligned} \tag{30}$$

The numerical solution and the exact solution at time $T = 0.5$ and $T = 0.7$ are shown in Fig. 4. Similar to the previous initial condition, the numerical results show that the present scheme can also obtain high resolution numerical solutions for this challenging examples with rich solution structures.

4.3 A junction with two incoming and one outgoing roads

This example involves an intersection that comprises of two entry roads, labelled as a and b, and one exit road, labelled c. Each of these roads is defined by the range $[0,1]$, as previously discussed in reference [2]. In our analysis, we refer to the two entry roads as Road1 and Road2, and the exit road as Road3, as depicted in Fig. 5. Accordingly,

$$\hat{\gamma}_c = \min\{\gamma_a^{\max} + \gamma_b^{\max}, \gamma_c^{\max}\}, \tag{31}$$

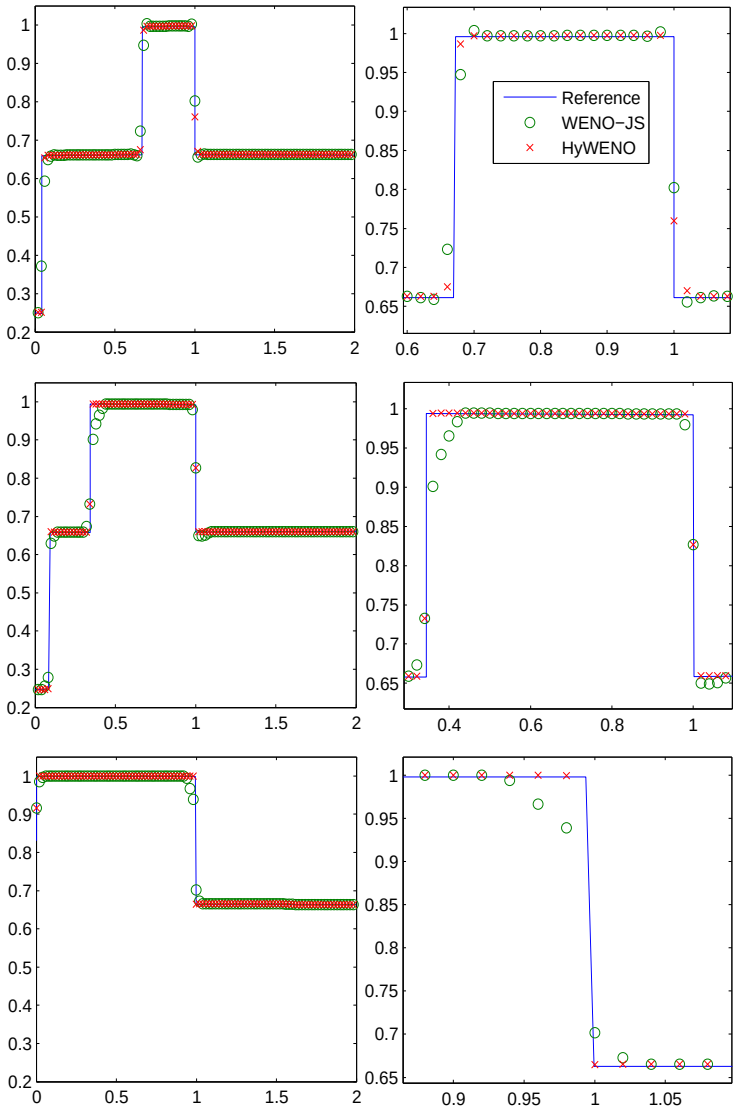

Figure 2: Bottleneck problem with initial data (28). Left (top to bottom): numerical solution with $N = 100$ at the final time $T = 0.5,\ 1.0$ and $T = 4.0$. Right: Zoomed region.

where the maximum flux $\gamma_a^{\max}, \gamma_b^{\max}$ and $\gamma_c^{\max}$ are defined as in (3). If $\gamma_a^{\max} + \gamma_b^{\max} \leq \gamma_c^{\max}$, then we set [4]

$$\hat{\gamma}_a = \gamma_a^{\max}, \hat{\gamma}_b = \gamma_b^{\max}, \hat{\gamma}_c = \hat{\gamma}_a + \hat{\gamma}_b. \tag{32}$$

For the case of $\gamma_a^{\max} + \gamma_b^{\max} > \gamma_c^{\max}$, it follows [4]

$$\begin{aligned}
&\hat{\gamma}_a = q\gamma_c^{\max}, \hat{\gamma}_b = (1-q)\gamma_c^{\max}, \hat{\gamma}_c = \gamma_c^{\max}, \text{ if } \gamma_a^{\max} \geq q\gamma_c^{\max}, \gamma_b^{\max} \geq (1-q)\gamma_c^{\max}, \\
&\hat{\gamma}_a = \gamma_a^{\max}, \hat{\gamma}_b = \gamma_c^{\max} - \gamma_a^{\max}, \hat{\gamma}_c = \gamma_c^{\max}, \text{ if } \gamma_a^{\max} < q\gamma_c^{\max}, \gamma_b^{\max} \geq (1-q)\gamma_c^{\max}, \\
&\hat{\gamma}_a = \gamma_c^{\max} - \gamma_b^{\max}, \hat{\gamma}_b = \gamma_b^{\max}, \hat{\gamma}_c = \gamma_c^{\max}, \text{ if } \gamma_a^{\max} \geq q\gamma_c^{\max}, \gamma_b^{\max} < (1-q)\gamma_c^{\max}.
\end{aligned} \tag{33}$$

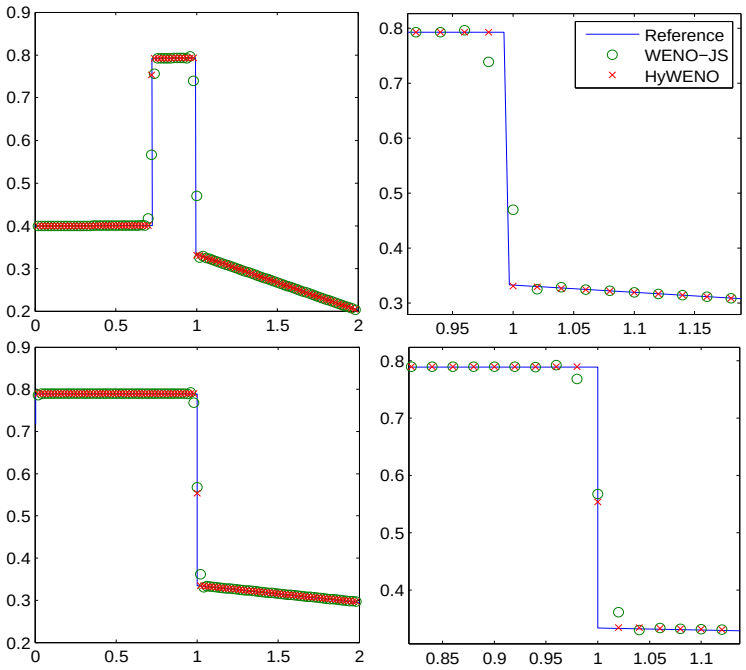

Figure 3: Bottleneck problem with initial data (29). Left (top to bottom): numerical solution with $N = 100$ at the final time $T = 4.0$ and $T = 10$. Right: Zoomed region.

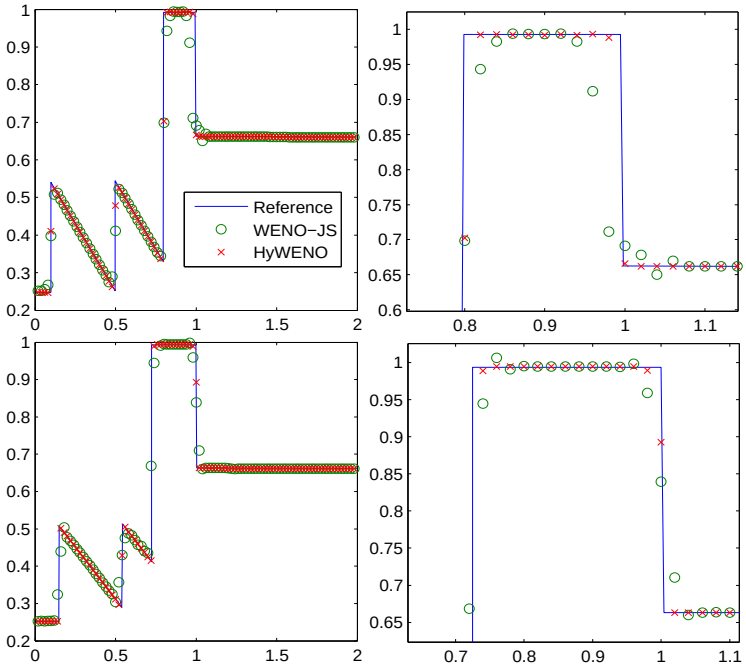

Figure 4: Bottleneck problem with initial data (30). Left (top to bottom): numerical solution with $N = 100$ at the final time $T = 0.5$ and $T = 0.7$. Right: Zoomed region.

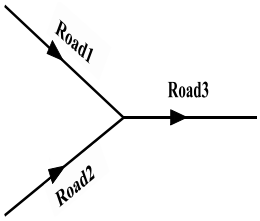

Figure 5: A junction with two incoming and one outgoing roads.

We make the assumption that drivers aim to maximize the flow of traffic through a junction. To facilitate this, the numerical fluxes for both incoming and outgoing roads at the junction point are set to a predefined value of

$$\hat{f}^K_{N+\frac{1}{2}} = \hat{\gamma}_K, \quad K \in \{a,b,c\}. \tag{34}$$

We are given the flux function for three roads: incoming road a, incoming road b, and outgoing road c, which are all described by (24). The following initial condition is considered

$$\begin{aligned}
\rho_1(x,0) &= \begin{cases} 0.1+0.1\sin^3(5\pi x), & x \in [0,0.2]\cup[0.4,0.6]\cup[0.8,1], \\ 0.2, & \text{otherwise.} \end{cases} \\
\rho_2(x,0) &= \begin{cases} 0, & x \in [0,0.2]\cup[0.4,0.6]\cup[0.8,1], \\ 0.1+0.1\sin(5\pi x), & \text{otherwise.} \end{cases} \\
\rho_3(x,0) &= 0.1.
\end{aligned} \tag{35}$$

Also, the boundary conditions are assigned as $\rho_{m,b}(0,t) = 0.1$ with $m = 1,2$. Fig. 6 displays the numerical and reference solutions for Road1 at time $T = 0.5$ and $T = 1.0$, using $N = 100$. The new scheme yields more precise numerical solutions than the classical fifth-order WENO-JS scheme, and it avoids spurious oscillations. Fig. 7 compares the numerical solutions of the new scheme and the WENO-JS scheme (with and without limiters) for Road2 at $T = 0.5$. When limiters are used, the numerical solutions are positive. However, without limiters, the minimum values are negative. Finally, Fig. 8 illustrates the numerical solutions for Road3 at $T = 0.5$ and $T = 1.0$ using $N = 100$. The new scheme yields more precise numerical solutions than the classical fifth-order WENO-JS scheme, and it avoids spurious oscillations.

4.4 A junction with two incoming and two outgoing roads

This instance involves a crossing that has two entryways, named a and b, and two exits, named c and d. Each of these roads is defined by the range $[0,1]$, as shown in Fig. 9. To simplify the computation, we refer to the incoming roads as Road1 and Road2, and the outgoing roads as Road3 and Road4. In this case, the traffic distribution matrix (2) can be rewritten as

$$\mathbf{A} = \begin{bmatrix} \alpha & \beta \\ 1-\alpha & 1-\beta \end{bmatrix},$$

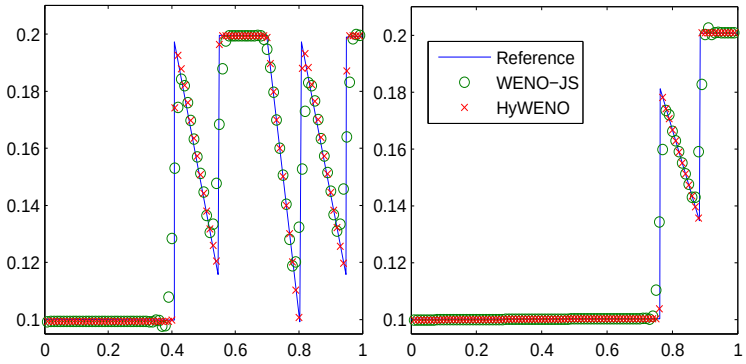

Figure 6: Two incoming and one outgoing roads with initial data (35) for Road1. Left: $T = 0.5$ and right: $T = 1.0$.

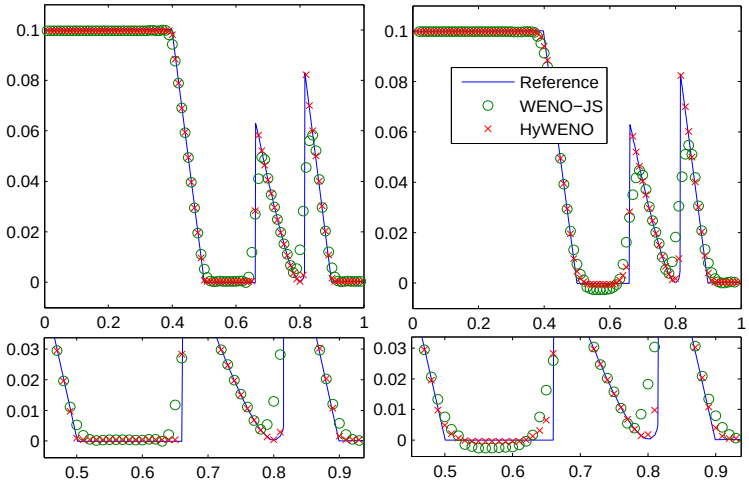

Figure 7: Two incoming and one outgoing roads with initial data (35) for Road2 at $T = 0.5$. Left: with limiter and right: without limiter.

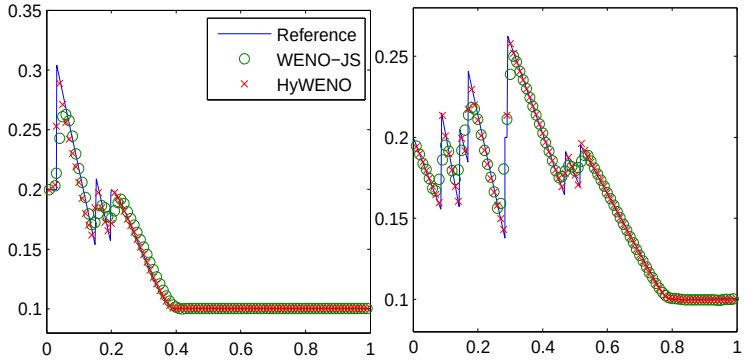

Figure 8: Two incoming and one outgoing roads with initial data (35) for Road3. Left: $T = 0.5$ and right: $T = 1.0$.

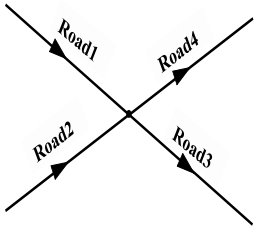

Figure 9: A junction with two incoming and two outgoing roads.

where $\alpha, \beta \in [0,1]$. We can guarantee the flux balance condition at junctions (2) with

$$\begin{bmatrix} \alpha & \beta \\ 1-\alpha & 1-\beta \end{bmatrix} \begin{bmatrix} \gamma_a \\ \gamma_b \end{bmatrix} = \begin{bmatrix} \gamma_c \\ \gamma_d \end{bmatrix}.$$

In order to find a unique solution for this situation, additional limitations are needed when choosing a particular incoming flux, such as $\hat{\gamma}_a$ and $\hat{\gamma}_b$. Additionally, we are assuming that the drivers will act in a manner that maximizes the outgoing flux, then

$$\alpha\gamma_a + \beta\gamma_b = \gamma_c^{\max}, \quad (1-\alpha)\gamma_a + (1-\beta)\gamma_b = \gamma_d^{\max}. \tag{36}$$

The numerical fluxes $\hat{\gamma}_a$ and $\hat{\gamma}_b$ at the junction point are expressed through various scenarios which are explained in detail in reference [4]:

I. if $\gamma_a \le \gamma_a^{\max}$ and $\gamma_b \le \gamma_b^{\max}$ therefore $\hat{\gamma}_a = \gamma_a,\ \hat{\gamma}_b = \gamma_b$;

II. if $\gamma_a > \gamma_a^{\max}$ and $\gamma_b > \gamma_b^{\max}$ therefore $\hat{\gamma}_a = \gamma_a^{\max},\ \hat{\gamma}_b = \gamma_b^{\max}$;

III. if $\gamma_a > \gamma_a^{\max}$ and $\gamma_b \le \gamma_b^{\max}$, if $\alpha < \beta$ therefore $\hat{\gamma}_a = \gamma_a^{\max},\ \hat{\gamma}_b = \min\left(\dfrac{\gamma_c^{\max} - \alpha\gamma_a^{\max}}{\beta}, \gamma_b^{\max}\right)$ otherwise $\hat{\gamma}_a = \gamma_a^{\max},\ \hat{\gamma}_b = \min\left(\dfrac{\gamma_d^{\max} - (1-\alpha)\gamma_a^{\max}}{1-\beta}, \gamma_b^{\max}\right)$;

IV. if $\gamma_a \le \gamma_a^{\max}$ and $\gamma_b > \gamma_b^{\max}$, if $\alpha > \beta$ therefore $\hat{\gamma}_b = \gamma_b^{\max},\ \hat{\gamma}_a = \min\left(\dfrac{\gamma_c^{\max} - \beta\gamma_b^{\max}}{\alpha}, \gamma_a^{\max}\right)$ otherwise $\hat{\gamma}_b = \gamma_b^{\max},\ \hat{\gamma}_a = \min\left(\dfrac{\gamma_d^{\max} - (1-\beta)\gamma_b^{\max}}{1-\alpha}, \gamma_a^{\max}\right)$.

The values of $\hat{f}^a_{N_a+\frac{1}{2}} = \hat{\gamma}_a,\ \hat{f}^b_{N_b+\frac{1}{2}} = \hat{\gamma}_b,\ \hat{f}^c_{\frac{1}{2}} = \hat{\gamma}_c,\ \hat{f}^d_{\frac{1}{2}} = \hat{\gamma}_d$ are assigned to the numerical fluxes at the point where incoming and outgoing roads intersect. Eq. (24) provides the flux function for both incoming and outgoing roads, and the distribution matrix is defined as

$$\mathbf{A} = \begin{bmatrix} 0.4 & 0.3 \\ 0.6 & 0.7 \end{bmatrix}.$$

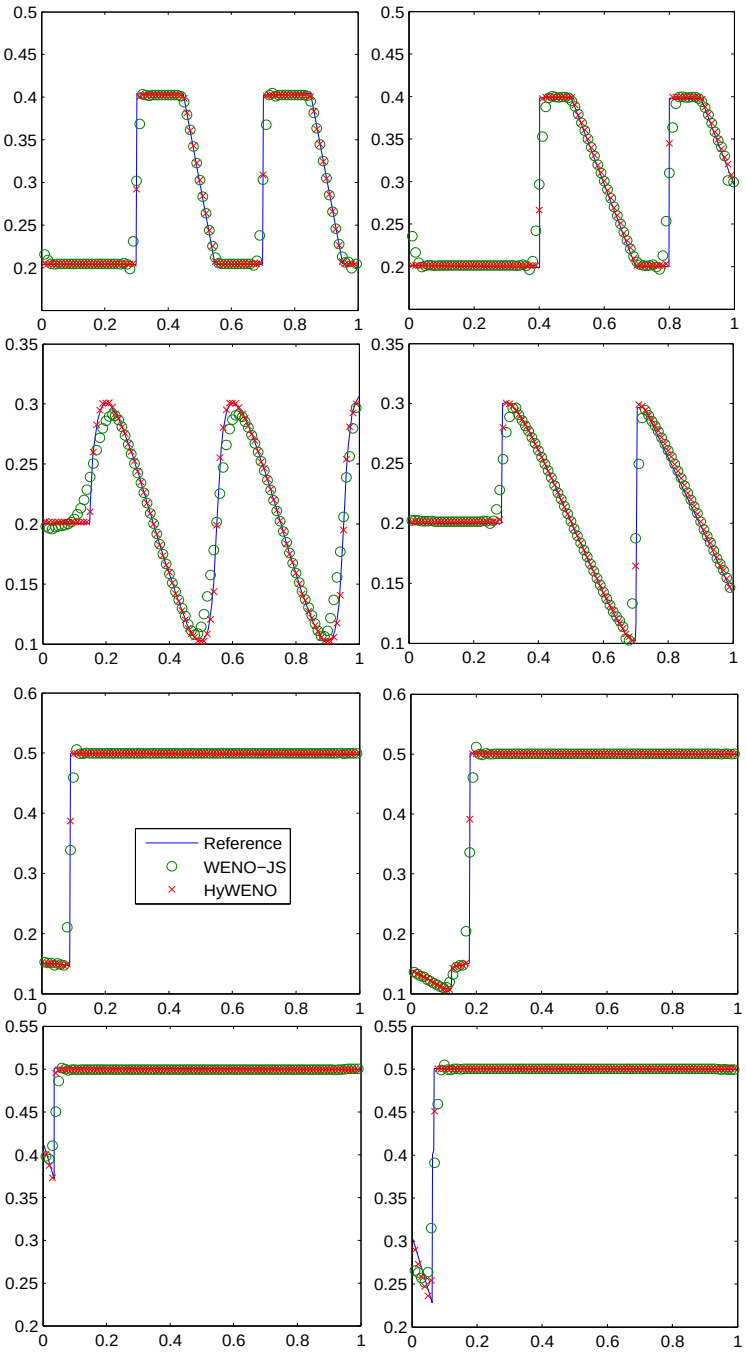

Figure 10: Two incoming and two outgoing roads with initial and boundary data (37). Left: $T = 0.25$ and right: $T = 0.5$. Top to bottom: Road1, Road2, Road3, and Road4.

The following initial condition and boundary condition are assigned

$$\begin{aligned}
&\rho_1(x,0) = \begin{cases} 0.2, & x \in [0,0.2] \cup [0.4,0.6] \cup [0.8,1], \\ 0.4, & \text{otherwise.} \end{cases} \\
&\rho_2(x,0) = 0.2 + 0.1\sin(5\pi x), \\
&\rho_3(x,0) = 0.5, \\
&\rho_4(x,0) = 0.5, \\
&\rho_{k,b}(0,t) = 0.2, \quad k = 1,2.
\end{aligned} \tag{37}$$

Fig. 10 displays the numerical solutions for Road1, Road2, Road3, and Road4 at two different times, specifically $T = 0.25$ and $T = 0.5$ using $N = 100$. The numerical solutions are characterized by high resolution and absence of oscillations, and are considered to be quite satisfactory.

5 Conclusions

In this research work, we developed a maximum-principle-satisfying non-linear high-order finite volume HyWENO scheme to traffic flow problem on networks. The finite volume HyWENO scheme is coupled with a limiter at each time stage to satisfy strict maximum principle under suitable CFL numbers, which would be important for traffic flow problems, where positivity of the density should be guaranteed. This was demonstrated on several examples, including those involving solutions with rich solution structures, where higher-order accuracy at edges and vertices of the traffic flow network provided superior solution quality. Extensions of the proposed algorithm to systems of hyperbolic conservation laws on networks are subject to future investigations.

Acknowledgment

The author is very thankful to the reviewers for carefully reading the paper, their comments and suggestions have improved the quality of the paper.

References

[1] R. Abedian, H. Adibi, M. Dehghan, *A high-order symmetrical weighted hybrid ENO-flux limiter scheme for hyperbolic conservation laws*, Comput. Phys. Commun. **185** (2014) 106–127.

[2] G. Bretti, R. Natalini, B. Piccoli, *Numerical approximations of a traffic flow model on networks*, Netw. Heterog. Media **1** (2006) 57–84.

[3] G. Bretti, R. Natalini, B. Piccoli, *A fluid-dynamic traffic model on road networks*, Arch. Comput. Methods Eng. **14** (2007) 139–172.

[4] S. Canic, B. Piccoli, J.-M. Qiu, T. Ren, *Runge-Kutta discontinuous Galerkin method for traffic flow model on networks*, J. Sci. Comput. **63** (2015) 233–255.

[5] G.M. Coclite, M. Garavello, B. Piccoli, *Traffic flow on a road network*, SIAM J. Math. Anal. **36** (2005) 1862–1886.

[6] C.F. Daganzo, *A behavioral theory of multi-Lane traffic flow. Part I: Long homogeneous freeway sections*, Transp. Res., Part B, Methodol. **36** (2002) 131–158.

[7] L. Fermo, A. Tosin, *A fully-discrete-state kinetic theory approach to traffic flow on road networks*, Math. Models Methods Appl. Sci. **25** (2015) 423–461.

[8] A. Harten, S. Osher, *Uniformly high-order accurate nonoscillatory schemes I*, SIAM J. Numer. Anal. **24** (1987) 279–309.

[9] H. Holden, N.H. Risebro, *A mathematical model of traffic flow on a network of unidirectional roads*, SIAM J. Math. Anal. **26** (1995) 999–1017.

[10] G.-S. Jiang, C.-W. Shu, *Efficient implementation of weighted ENO schemes*, J. Comput. Phys. **126** (1996) 202–228.

[11] M.J. Lighthill, G.B. Whitham, *On kinematic waves. II. A theory of traffic flow on long crowded roads*, Proc. R. Soc. Lond. Ser. A, Math. Phys. Sci. **229** (1955) 317–345.

[12] H. Liu, H. Xu, H. Gong, *Modeling the asymmetry in traffic flow (b): macroscopic approach*, Appl. Math. Model. **37** (2013) 9441–9450.

[13] X.-D. Liu, S. Osher, T. Chan, *Weighted essentially non-oscillatory schemes*, J. Comput. Phys. **115** (1994) 200–212.

[14] H. Nessyahu, E. Tadmor, *Non-oscillatory central differencing for hyperbolic conservation laws*, J. Comput. Phys. **87** (1990) 408–463.

[15] P. I. Richards, *Shock waves on the highway*, Oper. Res. **4** (1956) 42–51.

[16] G. Wong, S. Wong, *A multi-class traffic flow model – an extension of LWR model with heterogeneous drivers*, Transp. Res., Part A, Policy Pract. **36** (2002) 827–841.

[17] M. Zhang, C.-W. Shu, G.C. Wong, S. Wong, *A weighted essentially non-oscillatory numerical scheme for a multi-class Lighthill-Whitham-Richards traffic flow model*, J. Comput. Phys. **191** (2003) 639–659.

[18] P. Zhang, S. Wong, C.-W. Shu, *A weighted essentially non-oscillatory numerical scheme for a multi-class traffic flow model on an inhomogeneous highway*, J. Comput. Phys. **212** (2006) 739–756.

[19] X. Zhang, C.-W. Shu, *Maximum-principle-satisfying and positivity-preserving high-order schemes for conservation laws: survey and new developments*, Proc. R. Soc. A, Math. Phys. Eng. Sci. **467** (2011) 2752–2776.